

CLOSED-LOOP AERODYNAMIC FLOW CONTROL OF A FREE PITCHING AIRFOIL

Daniel P. Brzozowski

Graduate Research Assistant, Woodruff School of Mechanical Engineering
Georgia Institute of Technology, Atlanta, Georgia, USA, danb@gatech.edu

Michael E. DeSalvo

Graduate Research Assistant, Woodruff School of Mechanical Engineering
Georgia Institute of Technology, Atlanta, Georgia, USA

John R. Culp

Research Engineer II, Woodruff School of Mechanical Engineering
Georgia Institute of Technology, Atlanta, Georgia, USA

Ari Glezer

Professor, Woodruff School of Mechanical Engineering
Georgia Institute of Technology, Atlanta, Georgia, USA

ABSTRACT

Closed-loop feedback control of the attitude of a free pitching airfoil is effected without moving control surfaces by alternate manipulation of nominally-symmetric trapped vorticity concentrations on the suction and pressure surfaces near the trailing edge. The pitching moment is varied with minimal lift and drag penalties over a broad range of angles of attack when the baseline flow is fully attached. Accumulation (trapping) and regulation of vorticity is managed by integrated hybrid actuators (each comprised of a miniature $[O(0.01c)]$ obstruction and a synthetic jet actuator). In the present work, the model is trimmed using a position feedback loop and a servo motor actuator. Once the model is trimmed, the position feedback loop is opened and the servo motor acts like an inner loop control to alter the model's dynamic characteristics. Position control of the model is achieved using a reference model-based outer loop controller.

I. OVERVIEW

The aerodynamic effectiveness of lifting surfaces can be substantially improved by fluidic modification of their "apparent" shape through controlled interactions between arrays of surface-mounted synthetic jet actuators (Smith and Glezer 1998, Glezer and Amitay 2002) and the local cross flow that are also accompanied by local changes in the streamwise pressure gradients. These interactions lead to the formation of trapped vorticity concentrations where the balance between the trapped and shed vorticity is continuously regulated by the actuator jets. When the interaction domains are formed upstream of flow separation, the alteration of the local pressure gradients can result in complete or partial bypass (or suppression) of separation (e.g., Amitay et al. 1998, 2001 and Amitay and Glezer 2002, Glezer et al. 2005). Moreover, flow control by trapped vorticity is effective not only when the baseline

flow is separated but also when it is fully attached, namely at low angles of attack (i.e., at cruise conditions). This approach was exploited in the earlier works of Chatlynne et al. (2001) and Amitay et al. (2001) which showed that the formation of a stationary trapped vortex above an airfoil at low angles of attack leads to pressure drag reduction that is comparable to the magnitude of the pressure drag of the baseline configuration with minimal lift penalty. Actuation was accomplished using a hybrid actuator comprised of a synthetic jet downstream from a miniature surface-mounted passive obstruction of scale $O(0.01c)$ and the extent and strength of the trapped vortex was varied by varying the actuation frequency. Leveraging the presence of the miniature passive obstruction at low angles of attack drastically reduces the required actuation power compared to the use of the jet alone.

This approach was adopted by DeSalvo, Amitay, and Glezer (2002) and later by DeSalvo and Glezer (2004) to manipulate the Kutta condition of an airfoil using concentrations of trapped vorticity that are induced and controlled near the trailing edge by a hybrid actuator similar to a Gurney flap. From the standpoint of aerodynamic flow control, both L/D_p and the pitching moment, C_M , can be continuously adjusted by varying the actuation momentum coefficient over a broad range of angles of attack. The ensuing changes in the global flow near the trailing edge also result in a substantial reduction in drag (and therefore an increase in L/D_p) compared to both the baseline airfoil and the airfoil with inactive actuators. DeSalvo and Glezer realized an even greater decrease in pressure drag with virtually no loss in lift or significant change in skin friction drag by creating and manipulating trapped vorticity near the leading edge (2005) and more recently (2006) showed that similar actuation near the leading and trailing edges can lead to a significant simultaneous increase in lift and reduction in drag compared to the baseline airfoil.

Considerable progress in aerodynamic flow control in recent years has motivated the development of closed-loop flow control strategies for extending the flight envelope of flight vehicles and achieving dynamic maneuvering without mechanical control surfaces. While significant work on open-loop flow control has already demonstrated control effectiveness either on static or rigidly moving test platforms, relatively little work has been done on application of feedback control especially when the flow state is affected by the dynamic motion of the lifting surface as well as by the flow-control actuation. The implementation of feedback for modifying flow field characteristics requires appropriate sensing, actuation, and sufficient knowledge of the flow physics to achieve a desired aerodynamic performance state that would not occur naturally or be achievable with open loop control. Closed-loop approaches can enable greater performance, compensate for limited information about the flow state, provide robustness in the presence of noise, and adapt to changes in the behavior of the system or to failures in the actuators/sensors.

In the present work, closed-loop feedback control of a free-pitching airfoil is applied in wind tunnel experiments using bi-directional changes in the pitching moment that are effected by controllable, nominally-symmetric trapped vorticity concentrations on both the suction and pressure surfaces near the trailing edge. The actuation is effective with minimal lift penalty over a broad range of angles of attack and the aerodynamic characteristics of the airfoil can be continuously varied by alternate operation of the trailing edge actuators. The creation and manipulation of trapped vorticity in the vicinity of the actuator and its effect on the near wake are investigated in detail using particle image velocimetry (PIV) phase-locked to the actuation waveform.

II. EXPERIMENTAL SETUP

The present experiments use two airfoil models that span the width of the 1 x 1 m wind tunnel test section. Detailed measurements of the actuation effectiveness are conducted on a static swept (27° , $c_x = 501$ mm) fixed cross

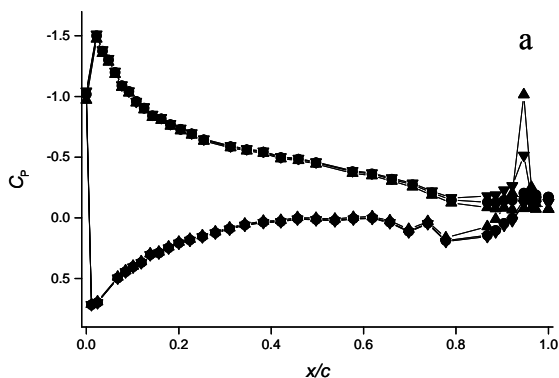


Figure 2 Pressure distribution around airfoil at $\alpha = 6^\circ$: (a) global view, and (b) trailing edge detail. Unactuated (\bullet), pressure surface (PS) actuator only (\blacktriangle), suction surface (SS) actuator only (\blacktriangledown), both actuators operating (\blacklozenge), and the baseline distribution ($-$).

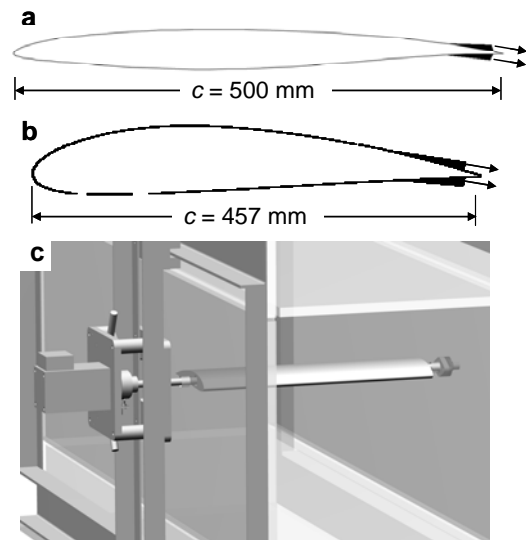


Figure 1 (a) Static (commercial) and (b) dynamic (NACA 4415) airfoil models with the integrated hybrid actuators near the trailing edge (the actuation jets are marked by arrows) used for static and dynamic measurements, respectively. c) The dynamic model and 1-DOF pitch traverse in the test section.

section airfoil model (based on a commercial aircraft configuration, Figure 1a). Dynamic measurements in pitch are obtained using a 2-D NACA 4415 airfoil model ($c = 457$ mm, $t/c = 0.15$) shown in Figure 1b. Each model is instrumented with a circumferential array of 70 pressure ports located at mid-span that are connected to an external high-speed pressure measurement system. Bi-directional, pitching moments induced by flow-control are effected by individually-controlled miniature, hybrid surface actuators integrated with rectangular, high aspect ratio synthetic jets that are surface-mounted on the pressure and suction surfaces of the airfoil upstream of the trailing edge ($x/c = 0.90$ and 0.95 , respectively for the static model in Figure 1a, and 0.96 for both surfaces of NACA 4415 in Figure 1b). The actuators have a characteristic height of $0.017c$ above the airfoil surface. The long dimension of the exit plane of each rectangular jet is parallel to the trailing edge and the cross stream width is 0.4 mm. The jets are generated by piezoelectric membranes that are built into a central cavity within the actuator and are operated within the range $1770 \text{ Hz} < f_{\text{act}} < 2350 \text{ Hz}$. The actuators are spanwise-segmented and are individually controlled from the laboratory computer and the system controller.

The dynamic model is mounted in the tunnel test section on a 1-DOF (pitch) traverse (Figure 1c) that is electromechanically driven by a dedicated feedback controller. A servo motor is directly coupled to the wing and is driven by a servo amplifier in torque mode to control the pitching moment on the wing from the system's controller. For open loop characterization experiments the traverse is used to enforce a prescribed time-dependent angle of attack (α) trajectory. It also serves as a virtual variable tail surface by providing the torque required to trim the wing at any given condition and modifying its dynamic characteristics by changing its stiffness and damping

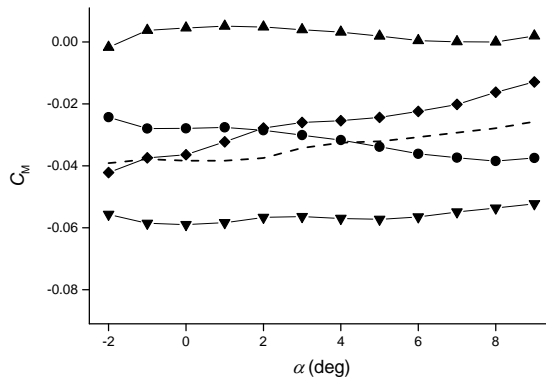


Figure 3 Variation of C_M with α . Symbols as in Figure 2.

properties. The application of torque that is proportional to α and $\dot{\alpha}$ effectively alters $\partial C_M / \partial \alpha$ and $\partial C_M / \partial \dot{\alpha}$. This allows for study of behavior and control of a range of ‘virtual’ air vehicles, all having the same wing as the wind tunnel model, but with different stability properties, including unstable configurations. It is also possible to use acceleration feedback to control the effective moment of inertia of the model. In addition, the servo motor is used as a transducer to indirectly measure the aerodynamic moment. In torque mode the motor generates a torque proportional to the input voltage. At steady state, the motor torque balances the aerodynamic moment and moment due to gravity which is removed using measurements in the absence of flow.

The bulk of the present experiments are conducted at a free stream speed of up to $U_\infty = 30$ m/s, with a corresponding Reynolds number based on the airfoil chord length of $Re_c = 1 \cdot 10^6$ (static airfoil) and $8.55 \cdot 10^5$ (dynamic airfoil). At this speed, the actuation Strouhal number $St = f_{act}c/U_\infty$ varies between 26 and 39 and the maximum momentum coefficient is $C_\mu = 1 \cdot 10^{-3}$.

III. OPEN LOOP AERODYNAMIC CONTROL ON A STATIC MODEL

One of the primary objectives of the present work is to demonstrate *bi-directional changes in the pitching moment*

of an airfoil at low angles of attack without the presence of moving control surfaces. The flow near the trailing edge is altered with minimal lift and drag penalties by leveraging the presence of controllable trapped vorticity concentrations on both the suction and pressure surfaces. The earlier work of DeSalvo and Glezer (2004, 2006) has shown that the operation of a hybrid actuator on the pressure surface near the trailing edge of an airfoil leads to a substantial change in the pressure distribution on the *opposite* surface which generates a nose-up pitching moment (relative to the unactuated configuration). Building on these findings, hybrid actuators are placed near the trailing edge on both the pressure side (*PS*) and suction side (*SS*) ($x/c = 0.95$ and 0.90 , respectively) to independently effect pitch-up or pitch-down moments.

Pressure distributions around the airfoil at $\alpha = 6^\circ$ (Figure 2) show that the operation of the pressure surface actuator leads to a pressure increase at the trailing edge of $\Delta C_p \approx 0.1$ (relative to the unactuated condition) that extends to the opposite surface and therefore leads to a pitch-up moment increment. Similar changes in the pressure distribution occur when the suction surface actuator is operated, producing an opposite, nose-down pitching moment. It is evident that the small concentration of trapped vorticity that is formed immediately downstream of the operating actuator produces a region of very low pressure near the actuator orifice that accelerates the flow along the actuated surface upstream of the actuator. The trapped vorticity concentration increases pressure downstream of the actuator and at the trailing edge. As a result, the Kutta condition is modified so that the flow on the opposite surface from the operating actuator (around the trailing edge) decelerates, leading to increased pressures and a corresponding pitching moment (cf. Figure 2). A further contribution to the pitching moment comes from reduced pressure immediately upstream of the active actuator.

The variation of C_M with angle of attack ($-2^\circ < \alpha < 9^\circ$) for the baseline airfoil and in the presence of the inactive and active actuators is shown in Figure 3. In the absence of actuation C_M decreases with α while C_{M0} (for the smooth airfoil) increases with α indicating that the inactive actuators render the airfoil slightly more stable as evidenced

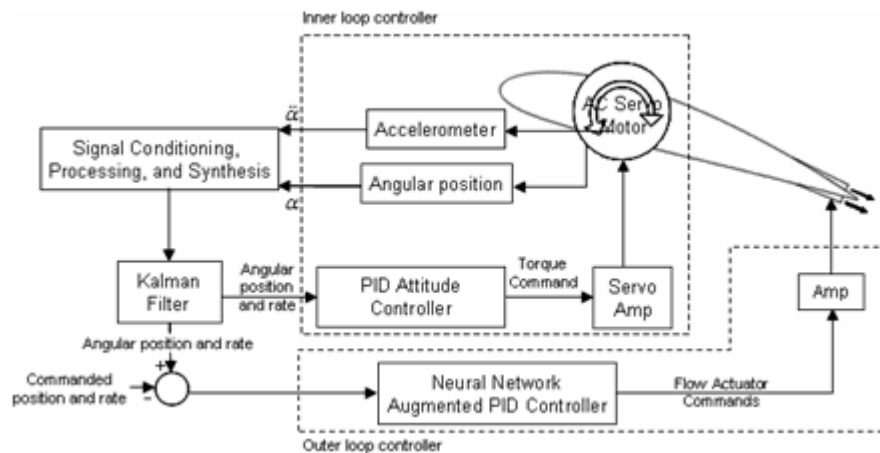


Figure 4 Pitching airfoil 1-DOF controller.

by the change in $\partial C_M / \partial \alpha$ compared to the smooth airfoil.

When either one of the actuators (*PS* or *SS*) is active, C_M varies only slightly with α . However, while the moment difference between these actuation conditions is also relatively invariant with α ($\Delta C_M = 0.058$), the moment increments induced by *PS* and *SS* actuation relative to the unactuated airfoil monotonically decrease and increase, respectively as α increases. For instance, at $\alpha = 8^\circ$, ΔC_M (with respect to the unactuated condition) for *PS* and *SS* actuation has respective values of +0.038 and -0.009. The ranges of C_M values that are achievable using actuation alone allow the moment coefficient to be varied between approximately the value of the smooth (unactuated) airfoil and a value corresponding to a (small) nose-up pitching moment. Simultaneous operation of both actuators produces a ΔC_M (with respect to the unactuated condition) of an amount nearly equal to the combination of the ΔC_M values of the individual actuators, indicating that the effects of the *PS* and *SS* actuators on C_M are independent of each other.

IV. CLOSED-LOOP FLOW CONTROL OF A FREE PITCHING AIRFOIL

A schematic diagram of the system controller is shown in Figure 4. The controller is comprised of two independent loops: an inner loop for the torque motor and an outer loop for the flow actuators. In normal operation (when the flow control actuators are activated) there are no external commands to the inner loop (servo motor control). The system with a closed inner loop controller (with no external commands) forms the plant for the flow control or outer loop. The angular position (angle of attack) and acceleration of the model are monitored using a position resolver and angular accelerometer. A Kalman filter blends the two signals to provide filtered angular position and rate information for both the inner and outer loop controllers. The inner loop controller is a PID controller in series with a linear dynamic compensator designed using the root locus approach and manual fine tuning on the experimental setup (Kutay et al, 2007). When the outer loop is in control, the inner loop controller switches to a complementary mode in

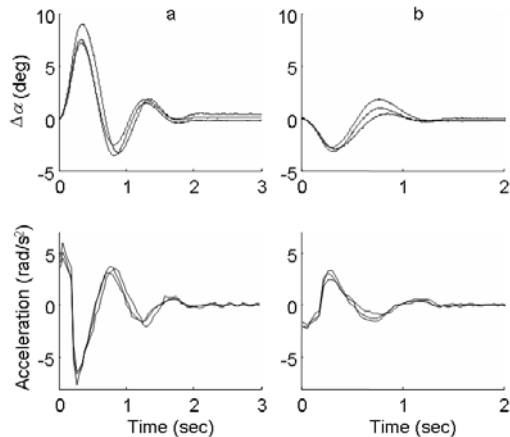


Figure 6 Open loop system response to a 0.2 sec impulse from the (a) *PS* and (b) *SS* actuators at $\alpha = -2^\circ, 0^\circ$, and 2° .

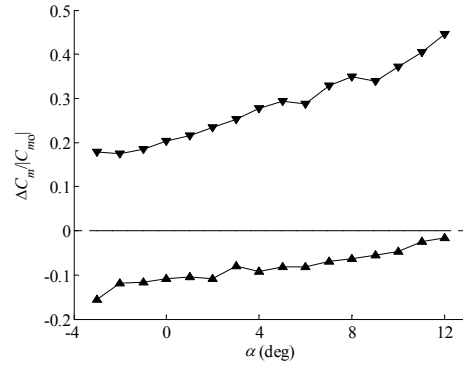


Figure 5 Variation of steady actuator effectiveness with angle of attack: \blacktriangle *SS* actuators, \blacktriangledown *PS* actuators.

which it sets the selected dynamic characteristics of the plant that the outer loop controller sees (e.g., desired stiffness and damping) and supplies the trim torque. At this state, only the outer loop controller responds to external commands and motion control is achieved exclusively through the flow control actuators. The output of the outer loop controller represents the commanded change in pitching moment and is analogous to commanded control of conventional control surfaces. Positive control signal indicates nose up moment and requires activation of the pressure side (*PS*) actuators and similarly negative control signal requires activation of the suction side (*SS*) actuators.

The baseline outer loop controller is a PID controller that is tuned based on experimental measurements. While the PID controller has satisfactory performance for the design model, its performance diminishes quickly as the model stability is reduced through the inner loop controller. In order to increase the robustness of the outer loop controller to changes in plant stability characteristics (e.g., due to varying flight conditions), the baseline PID controller can be augmented by an adaptive neural network controller.

For closed loop control it is necessary to have sufficient control authority for tracking the desired angle of attack trajectory. The steady actuator effectiveness is defined by:

$$\frac{\Delta C_m}{|C_{m0}|} = \frac{T_{act} - T_{no\ act}}{|T_{no\ act} - T_{gravity}|} \quad (1)$$

where T_{act} is the applied servo torque needed to trim when the flow control actuators are active, $T_{no\ act}$ is the applied servo torque needed to trim in the absence of flow control actuation, and $T_{gravity}$ is the torque due to gravity (measured in the absence of cross flow). The effectiveness of the actuation is characterized by operating the *SS* and *PS* actuators over a range of angles of attack ($-3^\circ < \alpha < 12^\circ$, Figure 5). Even though the flow over the airfoil is *fully-attached*, the effectiveness of the actuation varies with the upstream flow conditions as a result of variations in the streamwise pressure gradient, boundary layer thickness, flow direction, etc. The data in Figure 5 show that while generally the effectiveness of the *PS* actuators increases

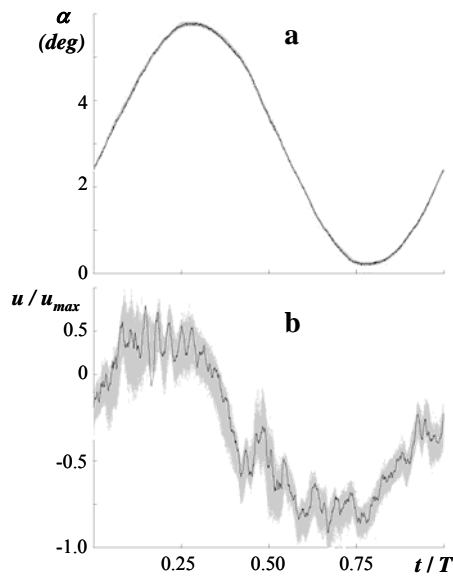


Figure 7 (a) Angle of attack and (b) actuator command signal for sinewave tracking with the outer loop. A single cycle is shown in black, 400 consecutive cycles are overlaid in gray. Dashed line shows desired trajectory.

with angle of attack, the effectiveness of the *SS* actuators decreases somewhat. This variation can be easily overcome by addressing either fewer *PS* actuators or operating them at lower actuation levels. It is remarkable that the moment increment between the *SS* and *PS* actuators remains substantially invariant below 8° , and that the *PS* actuators can achieve a moment increment as high as $0.45C_{M_0}$ at 12° .

The effectiveness of the actuators is also measured using impulse response. The wind tunnel model is brought to a desired attitude (angle of attack) using inner loop regulation and then the inner loop is opened so that the torque motor is used to simulate a tailed aircraft with no added damping. The *PS* and *SS* actuators are separately activated in a pulse modulated mode for 0.2 sec. Figure 6 shows the time history of the incremental change in angle of attack (relative to the nominal angle for $\alpha = -2^\circ, 0^\circ$, and 2°) and acceleration for the *PS* (Figure 6a) and *SS* (Figure 6b) actuators. These data show that following the actuation, the stable airfoil returns to its original angle of attack through damped oscillations at about 1 Hz. The maximum excursions in angle of attack for the *PS* and *SS* actuators are significant: about 7° and 3° , respectively and give an indication of the responsiveness of the present system under flow control actuation. The pulse response is very similar for the three nominal angles shown.

For the closed-loop flow control experiments, the attitude of the pitching airfoil is controlled with the outer loop controller using only the flow control actuators. For the design of the baseline controller, the inner loop controller provides a stable, well-damped system. The parameters of the PID controller are selected to yield reasonable response to a step input command. The ability of the controller to track a prescribed change in attitude in closed loop is demonstrated using a commanded 0.5 Hz sinusoidal variation in angle of attack for $0^\circ < \alpha < 6^\circ$.

Comparing the time-history of angle-of-attack with the commanded trajectory in Figure 7a, it is remarkable that the airfoil follows the desired trajectory with minimal phase delay and a deviation in angle of less than 0.2° . Furthermore, the controller is very repeatable over successive cycles with a standard deviation in angle that is below $\sigma_\alpha = 0.03^\circ$ throughout the cycle. The normalized flow control output, u/u_{max} , is shown in Figure 7b, where $u/u_{max} = \pm 1$ correspond to full-power actuation from the *PS* and *SS* actuators, respectively.

Since the maximum velocity of the airfoil's trailing edge is two orders of magnitude lower than the free stream velocity, it is reasonable to think of the flow motion as a quasi-steady process to which the results from the static airfoil can be applied. DeSalvo and Glezer (2004) showed previously that hybrid actuators of this type generate a pitching moment proportional to the power input which allows the controller to continuously vary the torque provided by the actuators to regulate the airfoil's attitude.

The fact that the control signal is not symmetric about zero is due to the fact that the *PS* actuators can effect a larger pitching moment than the *SS* actuators (cf. Figure 5) and therefore require less power. The *SS* actuators are engaged, providing a pitch-down moment, from $t/T = 0.05$ until $t/T = 0.35$. This corresponds to the portion of the cycle during which the airfoil is moving from $\alpha = 3^\circ$ through the maximum at $\alpha_{max} = 5.8^\circ$ and begins to pitch down again. The *PS* actuators are engaged during the remainder of the cycle.

The airfoil trajectory and control signal provides some insight into the nature of the forces that affect the airfoil during the cyclic pitch maneuver. For example, during the part of the cycle for which $\alpha > 3^\circ$, the airfoil experiences a nose-down acceleration which is strongest ($\ddot{\alpha}_{max} = -29^\circ/s^2$) at α_{max} . This would suggest nose-up moments acting on the airfoil from both the rigid-body motion as well as the "added mass" effect of accelerating the surrounding fluid. However, from the control signal it is evident that the actuators provide an additional nose-up pitching moment during this part of the cycle, suggesting that the dominant forces on the airfoil (not including the actuation) are nose-down. A complimentary analysis can be made for the remaining half of the cycle. One likely explanation for this

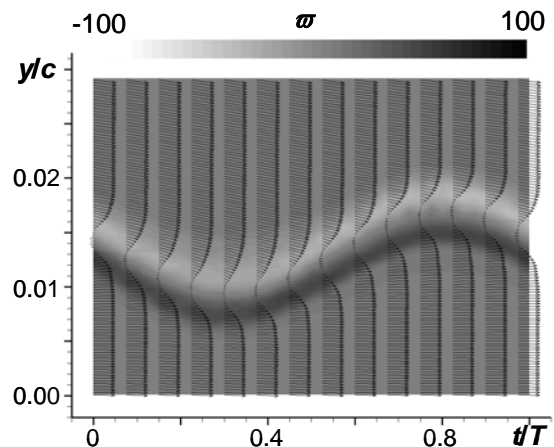


Figure 8 Time evolution of phase-averaged velocity (vectors) and vorticity (raster) in the wake.

behavior is the changing aerodynamic moment resulting from the center of pressure being located slightly away from the axis of rotation (quarter-chord).

The time evolution of phase-averaged vorticity in the wake is shown in Figure 8 with corresponding velocity vectors. The overall width of the wake and vorticity flux from either side of the airfoil remains invariant throughout the cycle. No significant dynamic effects are present as the peak velocity of the trailing edge (6 cm/s) is two orders of magnitude lower than the free stream velocity.

VI. CONCLUSIONS

The attitude of a free-pitching airfoil is controlled in wind tunnel experiments over a broad range of angles of attack when the baseline flow is fully attached in the absence of moving control surfaces. Control is effected using bi-directional pitching moment that is derived from flow-controlled trapped vorticity concentrations on the pressure and suction surfaces near the trailing edge when the baseline flow is attached. Vorticity is trapped and regulated using arrays of individually-controlled hybrid actuators integrated with synthetic jets [having momentum coefficient $C_{\mu} \sim O(10^{-3})$] to manipulate the domain of trapped vorticity that forms downstream of an $O(0.01c)$ obstruction.

The alteration of the aerodynamic forces and moments using bi-directional trailing edge actuation was investigated in detail on a static wind tunnel model. The manipulation of trapped vorticity concentrations alters the pressure distribution around the airfoil, allowing the pitching moment coefficient to be varied *bi-directionally*. The pressure (*PS*) and suction (*SS*) surface actuators induce relative pitch-up and -down moments, respectively. The present measurements show that the levels of C_M effected by the *PS* and *SS* actuators are reasonably independent of α over the range $-2^\circ < \alpha < 9^\circ$ and that the nominal range of moment values span $1.4C_{M_0}$ (where C_{M_0} is the moment of the smooth airfoil). Other measurements (not shown) have demonstrated that actuation can also be used to adjust C_L across a range of $\Delta C_L \approx 0.1$. While operation of the pressure side actuator leads to pressure drag levels that are comparable to the smooth airfoil and a slight reduction in lift (not shown), operation of the suction side actuator results in a small increase in pressure drag (17% at $\alpha = 6^\circ$ compared to the smooth airfoil) and a slight increase in lift.

In the present work, the model is trimmed using a position feedback loop and a servo motor actuator which acts like an inner loop control to alter the model's dynamic characteristics. The present system dynamics are such that the flow responds to actuation much faster than the vehicle which allows independent characterization of the flow response and vehicle dynamics. When flow control is engaged, position control of the model is achieved by an arbitrary reference model based adaptive outer loop controller that drives the flow actuators.

Future work will include development of integrated flow/vehicle controllers that utilize direct feedback of a subset of flow states for enhanced performance, and testing on a 2-DOF pitch and plunge wind tunnel traverse to study this technology in a more complex regime.

ACKNOWLEDGEMENT

This work has been supported in major part by AFOSR, monitored by Dr. Rhett Jefferies.

REFERENCES

- Amitay, M. and Glezer, A., "Controlled Transients of Flow Reattachment over Stalled Airfoils," International Journal of Heat Transfer and Fluid Flow, 23, 690-699, 2002.
- Amitay, M. and Glezer, A., "Flow Transients Induced on a 2D Airfoil by Pulse-Modulated Actuation," Experiments in Fluids, 40, 329, 2006.
- Amitay, M., Horvath, M., Michaux, M., and Glezer, A., "Virtual Aerodynamic Shape Modification at Low Angles of Attack using Synthetic Jet Actuators," AIAA Paper 2001-2975.
- Amitay, M., Smith, B. L., and Glezer, A., "Aerodynamic flow control using synthetic jet technology," AIAA-98-0208, 1998.
- Amitay, M., Smith, D. R., Kibens, V., Parekh, D. E., and Glezer, A., "Aerodynamic Flow Control over an Unconventional Airfoil Using Synthetic Jet Actuators," AIAA Journal 39(3), 361-370, 2001.
- Chatlynne, E., Rumigny, N., Amitay, M., and Glezer, A., "Virtual Aero-Shaping of a Clark-Y Airfoil using Synthetic Jet Actuators," AIAA Paper 2001-0732.
- DeSalvo, M., Amitay, M., and Glezer, A., "Modification of the Aerodynamic Performance of Airfoils at Low Angles of Attack: Trailing Edge Trapped Vortices," AIAA Paper 2002-3165.
- DeSalvo, M. and Glezer, A., "Aerodynamic Performance Modification at Low Angles of Attack by Trailing Edge Vortices," AIAA Paper 2004-2118.
- DeSalvo, M. and Glezer, A., "Airfoil Aerodynamic Performance Modification using Hybrid Surface Actuators," AIAA Paper 2005-0872.
- DeSalvo, M. and Glezer, A., "Aerodynamic Control at Low Angles of Attack using Trapped Vorticity Concentrations," AIAA Paper 2006-0100.
- DeSalvo, M. and Glezer, A., "Control of Airfoil Aerodynamic Performance Using Distributed Trapped Vorticity," AIAA-2007-0708, 2007.
- Glezer, A. and Amitay, M., "Synthetic Jets," Ann. Rev. Fluid Mech, 24, 2002.
- Glezer, A., Amitay, M., and Honohan, A., "Aspects of Low- and High-Frequency Actuation for Aerodynamic Flow Control," AIAA Journal 43(7), 1501-1511, 2005.
- Kutay, A. T., Calise, A. J., and Muse J. A., "A 1-DOF Wind Tunnel Experiment in Adaptive Flow Control," AIAA Guidance, Navigation, and Control Conference, Keystone, CO, 2006.
- Kutay, A. T., Culp, J., Muse, J., Brzozowski, D., Glezer, A., and Calise, A., "A Closed-Loop Flight Control Experiment Using Active Flow Control Actuators," AIAA-2007-0114, 2007.
- Smith, B. L. and Glezer, A., "The Formation and Evolution of Synthetic Jets," Physics of Fluids, 10, 1998.